DOE/ET-53088-434 IFSR #434

Strong and Weak Instabilities in a 4-D Mapping Model of Accelerator Dynamics

Tassos Bountis
Center for Statistical Mechanics and Complex Systems
and Institute for Fusion Studies
The University of Texas at Austin
Austin, Texas 78712

and

Stathis Tompaidis
Physics Department
The University of Texas at Austin
Austin, Texas 78712

May 1990

STRONG AND WEAK INSTABILITIES IN A 4–D MAPPING MODEL OF ACCELERATOR DYNAMICS

Tassos Bountis(*)
Center for Statistical Mechanics and Complex Systems
and Institute for Fusion Studies
The University of Texas at Austin
Austin, Texas 78712

and

Stathis Tompaidis
Physics Department
The University of Texas at Austin
Austin, Texas 78712

ABSTRACT

Periodic solutions of a 4-dimensional (4–D) mapping model of accelerator dynamics are obtained and their stability is studied. It is found that near such *unstable* periodic orbits of low period, there exist *chaotic* regions of strong instability in the 4–dimensional space x_n, x_{n+1}, y_n, y_{n+1}, through which orbits escape very quickly to infinity. On the other hand, near 2–dimensional orbits in the x_n, x_{n+1} plane (i.e., in the vicinity of "flat" beams with $y_n \equiv 0$) stability conditions are obtained for which the y_n oscillations do not grow appreciably even if x_1, x_0 are chosen within the chaotic layer of an associated unstable 2–D orbit. In the latter case, evidence of weak instabilities, or *Arnol'd diffusion* is found and diffusion coefficients are calculated ($\sim 10^{-11}$) and compared with the ones obtained ($\sim 10^{-19}$), when x_1, x_0 are chosen within a region of oscillatory (quasiperiodic) motion.

(*) Permanent Address: Mathematics Department, University of Patras, Patras 26110, Greece

I. Introduction

The stability of particle beams in high energy accelerators is a problem of great practical concern to which the methods and techniques of Nonlinear Dynamics are expected to make a significant contribution[1-6].

Two are the major types of nonlinear phenomena that can cause serious blow–up effects and significantly decrease the beams' luminosity, over short (strong instabilities) or long times (weak instabilities): The beam–beam interaction and sextupole (or higher multipole) nonlinearities due to residual currents in the super–conducting magnets.

The effects of the beam–beam interaction have been discussed by J. Tennyson and many other authors, in this and other volumes [1-4]. Particle transport through resonances, flip–flop, and other related phenomena have been analyzed, yielding appropriate tune and tune–shift values at which the beam–beam interaction should not pose a major threat to the safe operation of intersecting storage rings[1-4,6].

Particularly in the case of colliding $p-\bar{p}$ beams, (where radiation damping and quantum fluctuation effects may be considered negligible), even *weak instabilities* produced by Arnol'd diffusion[7], are not expected to significantly affect beam lifetimes[8]. *Strong instabilities* on the other hand (i.e., rapid escape of orbit, to infinity via large chaotic regions), simply do not occur in the beam–beam problem, since the beam–beam force drops to zero (as r^{-2}) away from the origin and particle orbits remain bounded apparently for all time[6,8].

In this paper, we shall treat the effect of sextupole nonlinearities on hadron beams passing through a FODO cell, composed of a dipole and two quadrupoles, focusing the particles' motion in the horizontal $(-x)$ and vertical $(-y)$ direction[5]. Unlike the beam–beam interaction, the (quadratric) nonlinear forces here increase "monotonically" in magnitude away from the origin and may cause strong (as well as weak) instabilities limiting significantly the beams' dynamical aperture.

Treating the sextupole nonlinearity as concentrated at *one point* in the cell, the dynamics of $p(\bar{p})$ particles passing through the cell, can be described by the Hamiltonian

$$H=\frac{1}{2}(p_x^2+p_y^2+q_x^2x^2+q_y^2y^2)+\epsilon(\frac{x^3}{3}-xy^2)\delta_{2\pi}(t), \tag{1}$$

where q_x, q_y are the betatron frequencies (or "tunes") in the x and y directions, ϵ is the strength of the nonlinearity and $\delta_{2\pi}(t)$ the 2π–periodic δ-function

$$\delta_{2\pi}(t)=\frac{1}{2\pi}\sum_{k=-\infty}^{\infty}\cos kt\ . \tag{2}$$

In this work, we shall actually work with the 4–dimensional (4–D) mapping to which Hamilton's equations derived from Eq. 1 *rigorously* reduce[9]:

$$x_{n+1}=2x_n\cos\omega_x-x_{n-1}-(\epsilon\sin\omega_x/q_x)(x_n^2-y_n^2) \tag{3a}$$

$$y_{n+1}=2y_n\cos\omega_y-y_{n-1}+(2\epsilon\sin\omega_y/q_y)x_ny_n \tag{3b}$$

describing the x_n, y_n displacements of the particle after its nth passage through the cell ($\omega_x = 2\pi q_x,\ \omega_y = 2\pi q_y$).

In section 2, we construct some fundamental m-periodic orbits of Eqs. 3 ($m = 3, 4, 5, \ldots$) in 4 dimensions, and find that when they are *unstable* (with respect to small perturbations) they have *large* chaotic regions about them through which particles can *escape to infinity* after a very small number of iterations.

On the other hand, in section 3, we show that weak instabilities can also occur near unstable 2-D orbits of Eq. 3a ($\hat{x}_n = \hat{x}_{n+m}, \hat{y}_n \equiv 0$). In particular, we find at some specific tune values that placing our initial x_1, x_0 within a chaotic layer of one such orbit, (small) y_n oscillations exhibit a slow amplitude growth that may be characterized as Arnol'd diffusion [7]. Diffusion coefficients for such a growth were calculated and found to be 8-9 orders of magnitude *larger* than the corresponding ones, obtained when x_1, x_0 are located near a stable 2-D orbit.

Finally, in section 4, we offer some concluding remarks and point out that the instabilities discussed in this paper need to be further studied in the presence of an additional factor, which is expected to *enhance* them and thus increase their damaging effect on the beams' life–time: This factor is the so–called *synchrotron oscillations*[1–4] occuring in the *longitudinal direction* (i.e., along the beam) due to the particles being accelerated in that direction by the rf cavities.

These oscillations are actually seen to produce a slow *modulation* in the horizontal and vertical oscillation frequencies of Eq. 1, which can be modelled by

$$q_{x,y} = q_{1,2}(1 + \lambda \cos \Omega t),\ |\lambda| << 1,\ \Omega << 1\ . \tag{4}$$

Thus, their overall effect may be studied by the theoretical methods of *modulation diffusion*, developed in recent years by Chirikov and co–workers[10]. This approach is currently under investigation and results are expected to appear in future publications[11].

2. 4–Dimensional Periodic Orbits and Stability

The transfer map for a particle's horizontal ($-x$) and vertical ($-y$) position and momentum variables, as it passes through a single FODO cell, may be written in the form[5]

$$\begin{pmatrix} x' \\ p'_x \\ y' \\ p'_y \end{pmatrix} = \mathrm{M} \begin{pmatrix} x \\ p_x + \frac{1}{2} k l_d (x^2 - y^2) \\ y \\ p_y - k l_d x y \end{pmatrix} \tag{5}$$

where k is the strength and l_d the length of the cell's dipole

$$\mathbf{M} = \mathbf{U}\,\mathbf{R}\,\mathbf{U}^{-1}\ ,\ \mathbf{U} = \begin{pmatrix} \mathbf{U}_x & \mathbf{O} \\ \mathbf{O} & \mathbf{U}_y \end{pmatrix}\ ,\ \mathbf{R} = \begin{pmatrix} \mathbf{R}(\omega_x) & \mathbf{O} \\ \mathbf{O} & \mathbf{R}(\omega_y) \end{pmatrix}$$

$$\mathbf{U}_{x,y} = \begin{pmatrix} \beta_{x,y}^{\frac{1}{2}} & 0 \\ \gamma_{x,y} & \beta_{x,y}^{-\frac{1}{2}} \end{pmatrix} \ , \ \mathbf{R}(\alpha) = \begin{pmatrix} \cos\alpha & -\sin\alpha \\ \sin\alpha & \cos\alpha \end{pmatrix} \tag{5a}$$

$\beta_{x,y}(s)$ are the betatron functions (s is the coordinate *along* the particle's ideal circular) path around the ring, $\gamma_{x,y} = \beta'_{x,y}(s)/2\beta_{x,y}^{-\frac{1}{2}}$, and

$$\omega_x = 2\pi q_x \ , \ \omega_y = 2\pi q_y \ , \tag{6}$$

q_x, q_y being the betatron frequencies or *"tunes"* of the x- and y-oscillations respectively, caused by the (linear) quadruple fields. Clearly, we have assumed in Eq. 5 that the sextupole nonlinearity is concentrated at the midpoint of the cell and serves to alter the momentum (but not the position) of the particle, by an instantaneous "kick".

Substituting Eq. 5a in Eq. 5 and eliminating the momentum variables p_x and p_y, we arrive after a little algebra, at the *second order* difference equations

$$\begin{aligned} x_{n+1} &= 2x_n \cos\omega_x - x_{n-1} - \frac{1}{2} k\, l_d \beta_x \sin\omega_x (x_n^2 - y_n^2), \\ y_{n+1} &= 2y_n \cos\omega_y - y_{n-1} + k\, l_d \beta_y \sin\omega_y x_n y_n \ , \end{aligned} \tag{7}$$

$n = 0, 1, 2, \ldots$, yielding the *new* x_{n+1} , y_{n+1} displacements after the nth passage of the particle through the cell (and its nth rotation around the ring).

Even though the betatron functions β_x, β_y are periodic functions of the distance s along the ring, they do not significantly vary about their mean values, so we may take

$$\beta_{x,y} = L/(2\pi q_{x,y}) = R_{eff} q_{x,y}^{-1} \tag{8}$$

where L is the length of the circumference and R_{eff} the effective radius of the ring. Defining now

$$c_{x,y} \equiv \cos\omega_{x,y} \quad , \quad s_{x,y} \equiv \sin\omega_{x,y} \ , \tag{9}$$

and

$$A = 2(k\, l_d \beta_y\, s_y)^{-1} \quad , \quad B \equiv 2(k^2 l_d^2 \beta_x \beta_y s_x s_y)^{-\frac{1}{2}} \ , \tag{10}$$

we can scale our x_n, y_n variables to

$$x_n = AX_n \quad , \quad y_n = BY_n \tag{11}$$

and rewrite our mapping equations in the simplified form

$$X_{n+1} = 2c_x X_n - X_{n-1} - \rho X_n^2 + Y_n^2 \ , \tag{12a}$$

$$Y_{n+1} = 2c_y Y_n - Y_{n-1} + 2X_n Y_n \ , \tag{12b}$$

with

$$\rho \equiv \beta_x s_x / \beta_y s_y \ . \tag{12c}$$

Note that Eqs. 12 constitute a 4–dimensional mapping

$$\mathbf{X}_{n+1} = T(\mathbf{X}_n) \quad , \quad \mathbf{X}_n \equiv (X_n, X_{n-1}, Y_n, Y_{n-1}) \; , \tag{13}$$

with only two parameters $q_x,\ q_y$.

The variational equations of this mapping about an orbit $\hat{\mathbf{X}}_n$ are found by substituting $\mathbf{X}_n = \hat{\mathbf{X}}_n + \mathbf{\Delta X}_n$ in Eq. 13 and linearizing

$$\mathbf{\Delta X}_{n+1} = \mathbf{J}(\hat{\mathbf{X}}_n)\mathbf{\Delta X}_n \; , \tag{14}$$

where $\mathbf{J}(\hat{\mathbf{X}}_n)$ is the Jacobian matrix of T. Clearly, since $|c_{x,y}| \leq 1$, cf. Eq. 9, the origin $\hat{\mathbf{X}}_n = \mathbf{O}$ is (linearly) stable for all q_x, q_y.

We now seek periodic orbits of Eq. 12 in the form of Fourier polynomials[12],

$$X_n = \sum_k A_k e^{i\omega kn} \quad , \qquad Y_n = \sum_k B_k e^{i\omega kn} \; , \tag{15}$$

with frequency

$$\omega/2\pi = m_1/m_2 \quad , \quad -\pi < \omega \leq \pi \; , \tag{16}$$

where k in Eq. 11 takes integer values such that

$$-\pi < k\omega \leq \pi \quad , \text{ or } \quad -\frac{m_2}{2} < km_1 \leq \frac{m_2}{2} \; .$$

Substituting Eq. 15 in Eq. 12 we obtain algebraic equations for the coefficients $A_k,\ B_k$:

$$\begin{aligned}
(\cos k\omega - \cos\omega)A'_k &= A_k(c_x - \cos\omega) - \frac{\rho}{2}\sum_l A_l A_{k-l} + \frac{1}{2}\sum_l B_l B_{k-l}, \\
(\cos k\omega - \cos\omega)B'_k &= B_k(c_y - \cos\omega) + \sum_l A_l B_{k-l} \; ,
\end{aligned} \tag{17}$$

which may be solved recursively from the left had side for $A'_k,\ B'_k$ for all $k \neq 1$. Of course, Eqs. 17 can also be solved in their original form ($A'_k = A_k \; , \; B'_k = B_k$) by an appropriate Newton algorithm.

Since we shall be interested in low period solutions, $m_1 = 1,\ m_2 = m$ in Eq. 16, and

$$\omega = 2\pi/m \quad , \quad m = 3, 4, 5 \ldots \tag{18}$$

we will solve Eq. 17 by iterative schemes[12,13], which are generally rapidly convergent. For example, for period $m = 3$ orbits we shall have to solve 4 equations for $A_0,\ |A_1|,\ B_0$ and $|B_1|$ of the form:

$$
\begin{aligned}
3A_0' &= A_0(2c_x+1) - \rho(A_0^2 + 2|A_1|^2) + B_0^2 + 2|B_1|^2, \\
3B_0' &= B_0(2c_y+1) + 2[A_0B_0 + 2|A_1|\,|B_1|\cos(\theta-\phi)], \\
0 &= |A_1|(2c_x+1) - 2\rho A_0|A_1| + 2\sigma_1^{-1}B_0|B_1| - \rho\sigma_2|A_1|^2 + \sigma_3|B_1|^2, \\
0 &= |B_1|(2c_y+1) + A_0|B_1| + \sigma_1|A_1|B_0 + \sigma_3|A_1|\,|B_1|,
\end{aligned} \tag{19}
$$

where

$$
A_1 = |A_1|e^{i\theta} \quad , \quad B_1 = |B_1|e^{i\phi} \tag{20a}
$$

and

$$
\sigma_1 = e^{i(\theta-\phi)} \quad , \quad \sigma_2 = e^{-3i\theta} \quad , \quad \sigma_3 = e^{-i2\phi - i\theta} \tag{20b}
$$

Now, there are several choices of ϕ, θ that correspond to *real* σ_1, σ_2 and σ_3 in Eq. 19 and some of them yield different period–3 orbits of the mapping. For example, for

$$
q_x = 0.425 \quad , \quad q_y = 0.344 \tag{21}
$$

(i) $\theta = 0\,, \phi = \pi/2$, yields the *stable* periodic orbits at the centers of the "islands" in Figure 1.

(ii) $\theta = \phi = \pi/3\,,$ gives the *unstable* period–3 orbits between the "islands" in Fig. 1

The stability of these orbits is determined by the eigenvalues of the return Jacobian matrix

$$
\mathbf{J}_m = \prod_{n=1}^{m} \mathbf{J}(\hat{X}_n) \tag{22}
$$

$m = 3$. As is well known, these eigenvalues must all lie on the unit circle for the m–periodic orbit to be stable[14].

There is a *strong instability* associated with these simple periodic orbits (or, low order *resonances*) of Eq. 12. When particles enter into their chaotic regions they are seen to escape very quickly to infinity. Thus the locations of these low period unstable orbits provide useful estimates of distances from the origin (in the X_n, X_{n+1}, and Y_n, Y_{n+1} planes) where this strong instability occurs.

We have similarly constructed period 4 ($\omega = \pi/2$) solutions of the mapping given by Eqs. 12. One of them, for example, was found to be stable for

$$
q_x = 0.235 \quad , \quad q_y = 0.230 \tag{23}
$$

at significantly large distances from the origin in both the X_n, X_{n+1} and Y_n, Y_{n+1} planes (see Figure 2a). This orbit was also obtained with the choice $\theta = 0$, $\phi = \pi/2$

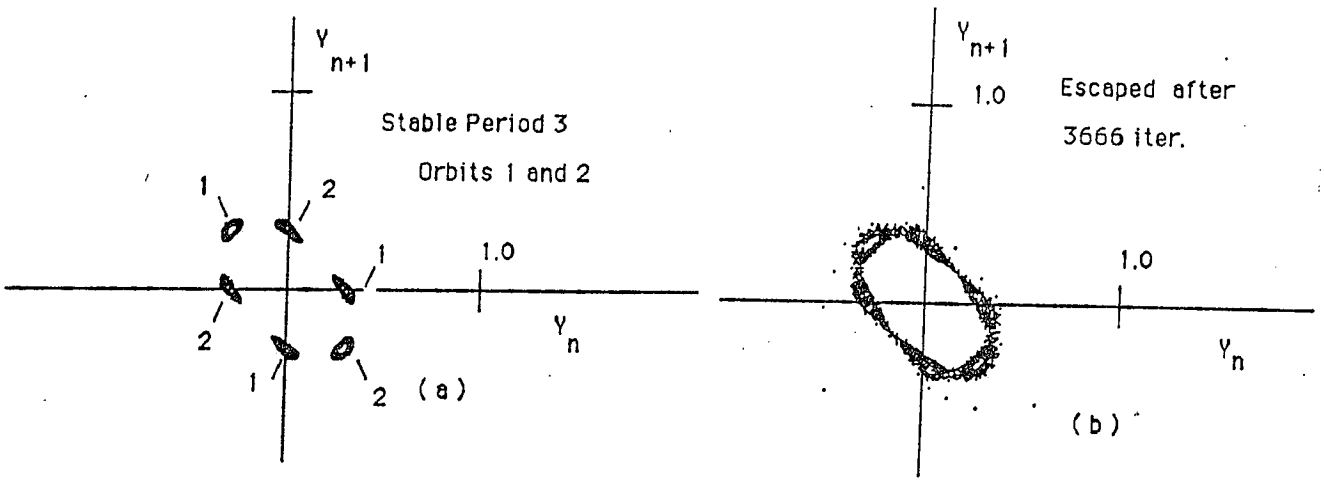

Figure 1(a). Stable period 3 orbit of the 4–D map at the centers of the "islands" marked by 1 (and its symmetric one, $Y_n \to -Y_n$, marked by 2), for initial conditions $X_0 = -.065$, $X_1 = .057$, $Y_0 = .02$, $Y_1 = -.31$; (b) Changing to $Y_0 = .04$, $X_1 = .06$ leads to rapid escape through the chaotic regions of the unstable period 3 orbits lying between the "islands". In both cases, $q_x = .425$, $q_y = .344$.

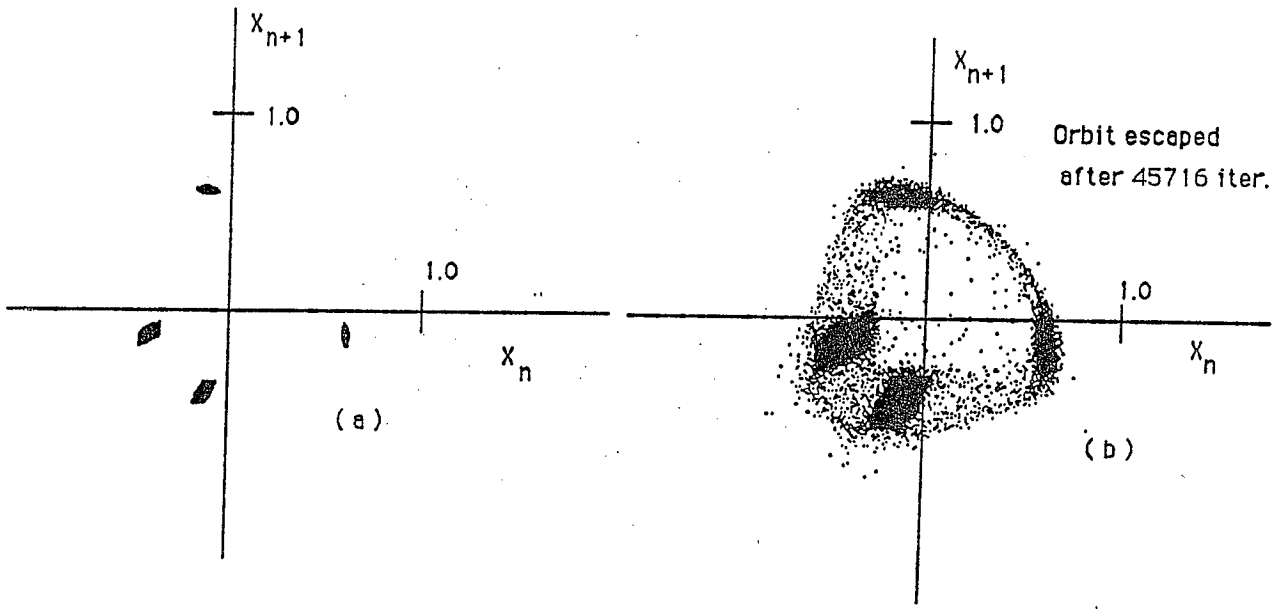

Figure 2. Same as Fig. 1 for motion near 4–D orbits of period 4 at $q_x = .235$, $q_y = .23$. (a) $X_0 = .6$, $X_1 = -.1$, $Y_0 = .01$, $Y_1 = -.5$ and no escape up to 10^6 iterations is observed; (b) Same as (a) but with $Y_0 = .05$: Escape occured a few hundred iterations after the orbit entered the chaotic region.

in its main Fourier coefficients of Eq. 20a, and has $B_0 = B_2 = 0$. As in the case of the period 3 orbit, when the initial conditions were such that particles eventually entered the chaotic region between the "tori", orbits were soon thereafter seen to escape to infinity, as shown, e.g. in Fig. 2b.

It is interesting to note what the intersections (projections) of 4–D tori about these periodic orbits look like in the X_n, X_{n+1} and/or Y_n, Y_{n+1} planes: In Figures 3 and 4 we show some of these "tori" associated with the period 3 and 4 orbits discussed above. As initial conditions are chosen further and further away from the periodic orbits these 4–D tori projections (which look remarkably like 2–dimensional tori!) grow in size and become more "jagged" and complicated in structure. It will take, however, further study before reliable statements can be made about how (and whether!) these tori actually "break-up" and "join" allowing orbits to rapidly run away to infinity.

3. Arnol'd Diffusion Near an Unstable 2–D Periodic Orbit

Long term orbital stability is not observed only near the origin and stable 4–D periodic orbits of our Eqs. 12. It can also be found near *stable 2–D m*-periodic solutions of Eq. 12a, $\{\hat{X}_n\}$, with $\hat{X}_n = \hat{X}_{n+m}$ and $\hat{Y}_n \equiv 0$. At the q_x values, however, where such solutions exist, q_y must be so chosen that small Y_n perturbations about these solutions *do not grow* exponentially via the parametric driving of $\hat{X}_n$ in Eq. 12b.

Suppose $\{\hat{X}_n\}$ is an m-periodic orbit of Eq. 12a, with $Y_n \equiv 0$. It is known that it will be (linearly) stable in 2–D as long as the following condition is satisfied [15]

$$|2 + \det \mathbf{H}_x| < 2 \tag{24}$$

where $\mathbf{H}_x$ is the $m \times m$ matrix with:

$$\begin{aligned} (\mathbf{H}_x)_{ii} &= 2c_x - 2\rho\hat{X}_i \quad , \quad i = 1, 2, \ldots, m\,, \\ (\mathbf{H}_x)_{i,i+1} &= (\mathbf{H}_x)_{i+1,i} = (\mathbf{H}_x)_{1,m} = (\mathbf{H}_x)_{m,1} = -1\,, \end{aligned} \tag{24a}$$

and all other elements zero.

This criterion was derived[15] from a Floquet type analysis of the *linearized* Eq. 12a (with $Y_n = 0$) about the m-periodic orbit $\{\hat{X}_n\}$. But the second equation of our 4–D mapping, Eq. 12b, is also *linear* in the Y_n and may be viewed, for small Y_n, as parametrically driven by the 2–D m-periodic solution $\{\hat{X}_n\}$ of Eq. 12a. We can therefore apply the same criterion as above to ensure that small Y_n oscillations about this 2-D periodic orbit remain bounded for very long times,

$$|2 + \det \mathbf{H}_y| < 2\,, \tag{25}$$

where $\mathbf{H}_y$ is the same matrix as as $\mathbf{H}_x$, except for its diagonal elements:

$$(\mathbf{H}_y)_{ii} = 2c_y + 2\hat{X}_i \quad , \; i = 1, 2, \ldots, m. \tag{25a}$$

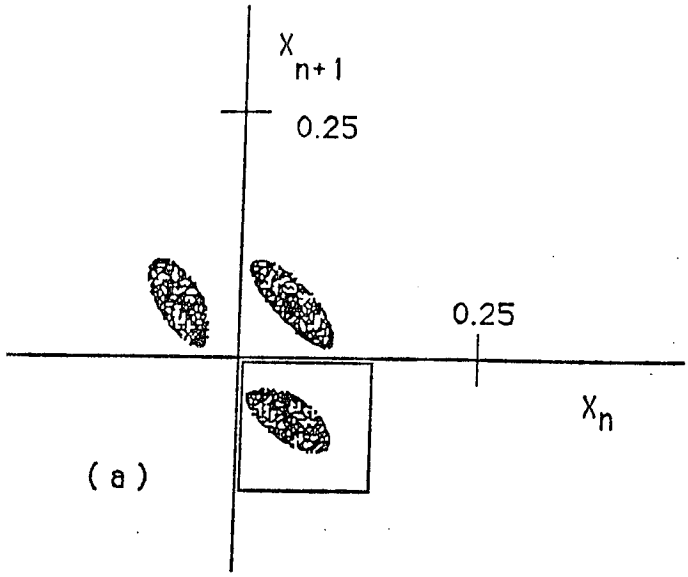

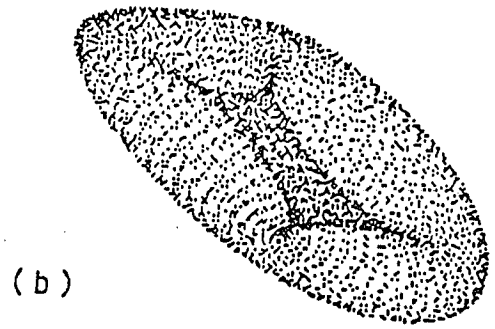

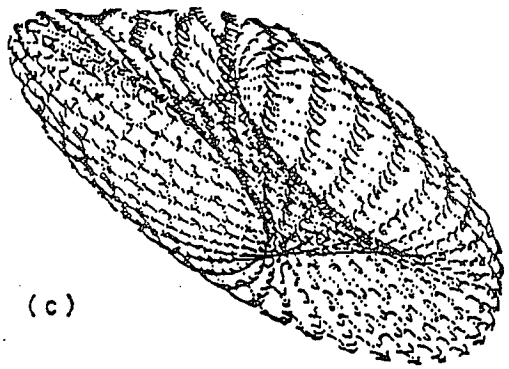

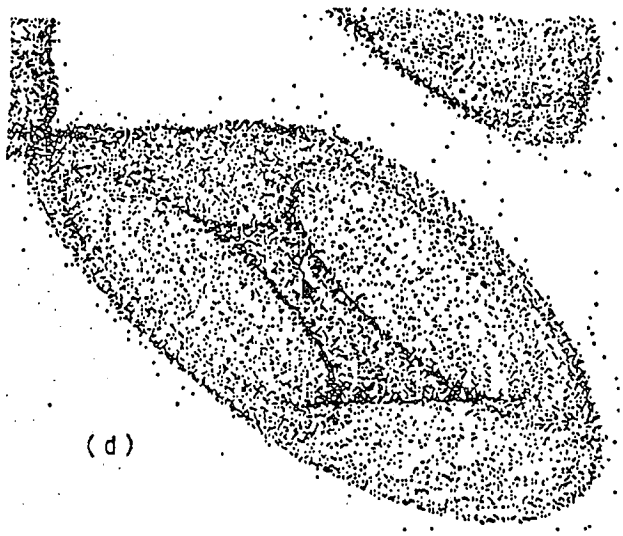

Figure 3.

(a) The stable period 3 orbit marked by 1 in Fig. 1(a), at $q_x = .425$, $q_y = .344$, in the X_n, X_{n+1} plane.

(b) A magnification of the 4–D torus in the box of (a), at the same initial conditions as in Fig. 1(a).

(c) Increasing only the Y_0 initial condition to $Y_0 = .03$ we observe that the tori grow in size and become more "irregular" in appearance.

(d) At $Y_0 = .0345$, the orbit stays for a long time on the tori, filling them out in an even more irregular and non-uniform way than (c) and eventually escapes after 28527 iterations of the map.

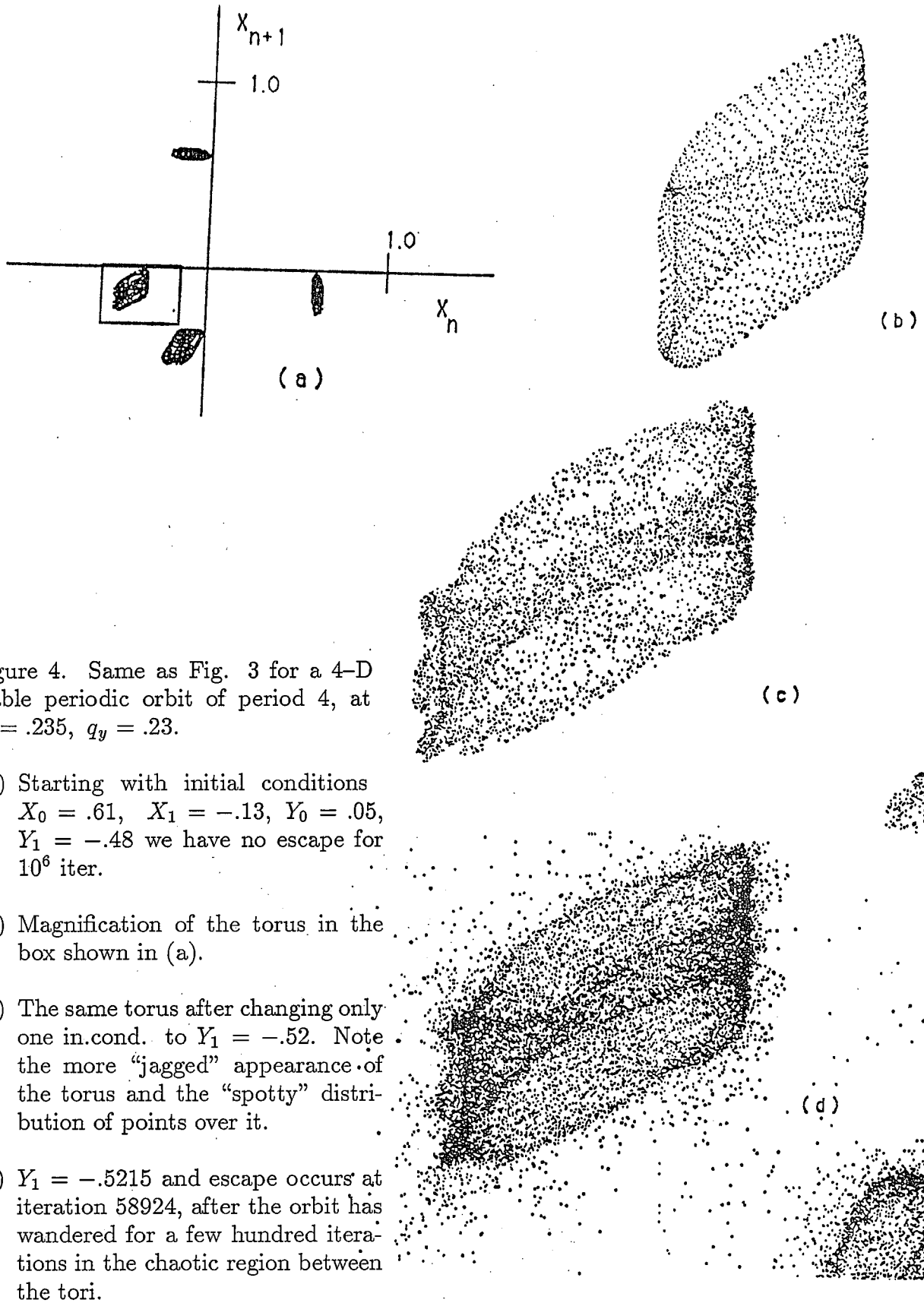

Figure 4. Same as Fig. 3 for a 4–D stable periodic orbit of period 4, at $q_x = .235$, $q_y = .23$.

(a) Starting with initial conditions $X_0 = .61$, $X_1 = -.13$, $Y_0 = .05$, $Y_1 = -.48$ we have no escape for 10^6 iter.

(b) Magnification of the torus in the box shown in (a).

(c) The same torus after changing only one in.cond. to $Y_1 = -.52$. Note the more "jagged" appearance of the torus and the "spotty" distribution of points over it.

(d) $Y_1 = -.5215$ and escape occurs at iteration 58924, after the orbit has wandered for a few hundred iterations in the chaotic region between the tori.

Thus, all we need to do to ensure long term stability in this case is look for q_x, q_y values such that the above two Ineqs. 24 and 25 are simultaneously satisfied.

Consider, for example, period 3 solutions of Eq. 12a (with $Y_n = 0$). Ineq. 24 gives in this case

$$1 < (4c_x^2 - 8c_x - 3)(1 + \sqrt{c_x^2 - 2c_x - 1}) < 3$$

or

$$0.318 \leq q_x \leq 0.333 \quad , \tag{26}$$

in order that these solutions be stable with respect to small variations in X_n. On the other hand, Ineq. 25 implies that small Y_n variations about these orbits will remain bounded provided

$$|4\left(c_y + \frac{c_x - a}{\rho}\right)^2 \left(c_y + \frac{1 + c_x + a}{\rho}\right) - 3c_y - \frac{3c_x + 1 - a}{\rho}| < 1 \ , \tag{27}$$

$a \equiv (c_x^2 - 2c_x - 1)^{\frac{1}{2}}$. Ranges of q_y values obtained from Ineq. 27 for different q_x satisfying Ineq. 26 are listed in Table 1 below.

Similar results are obtained for other m-periodic 2–D solutions of Eq. 12a: For $m = 5$, we have determined from Ineq. 24 that stability with respect to X_n-variations requires

$$0.21 \leq q_x \leq 0.229 \tag{28}$$

while for Y_n-boundedness, the corresponding intervals of q_y values obtained from Ineq. 25 are listed in Table 1 also.

Table 1
q_x, q_y Stability Intervals Near m–Periodic 2–D Orbits

m	q_x	q_y–Interval
3	0.320	(0, 0.12) and (0.387, 0.473)
	0.322	(0.390, 0.468)
	0.326	(0.396, 0.461)
	0.330	(0.400, 0.456)
5	0.210	(0.12, 0.16) and (0.2, 0.363)
	0.220	(0.195, 0.330)
	0.225	(0.185, 0.312)
	0.229	(0.180, 0.295)

Placing our X_1, X_0 initial conditions for the above q_x, q_y values near the stable 2–D orbits, we observed that orbits with Y_1, Y_0 small enough (typically $|Y_{0,1}| \sim 10^{-2}$) remained *bounded*, i.e., $X_n^2 + Y_n^2 < 1$, for 10^6 iterations of Eqs. 12. We also

observed that, for each q_x, the $Y_{\max} = \max\{|Y_0| + |Y_1|\}$ for stability varies over the corresponding q_y interval, attaining its largest values ($Y_{\max} \sim 0.1$) near the center of that interval.

And now we come to our evidence of *weak instabilities*, or Arnol'd diffusion in this model: Choosing initial conditions for X_0, X_1 at the point A, within the chaotic layer of the unstable 2–D period 5 orbit of Fig. 5a, we found that the Y_n oscillations—no matter how small their Y_1, Y_0—kept *growing* in amplitude (on the average) producing in the Y_n, Y_{n+1} plane a set of point *scattered* over a figure of intersecting "rings", as shown in Figs. 5b,c.

On the other hand, an orbit starting at a point B in Fig. 5a, within the period 5 islands, exhibited considerably *weaker* outward diffusion properties and produced a set of intersections lying on a much more clearly defined "ring"–pattern in the Y_n , Y_{n+1} plane (see Fig. 5d).

In an attempt to quantify these observations we followed a method due to Chirikov et al.[7,16] and divided our total number of iterations $N = 10^6$ into

1) $N_1 = 100$ subintervals of length $\Delta N_1 = 10,000$, and
2) $N_2 = 10$ subintervals of length $\Delta N_2 = 100,000$.

Then for each of these cases we computed the *diffusion coefficient*

$$D_k = \frac{2}{N_k(N_k-1)} \sum_{m>l} \frac{[\bar{Y}(m) - \bar{Y}(l)]^2}{(\Delta N_k)(m-l)} \ , \qquad k = 1,2 \tag{29}$$

$\bar{Y}(m)$ being the average of Y_n over the mth subinterval, $m,\ l = 1, 2, \ldots N_k$. (In Eq. 29 we have used $\bar{Y}(m)$ instead of the more common average of the Hamiltonian $\bar{H}(m)$[7,16] because, in our system, diffusion phenomena are more pronounced in the Y_n direction).

For a true diffusion process it should not matter if the motion is averaged over different numbers of subintervals, and hence one should expect:

$$D_1 \approx D_2 \qquad \text{(for Arnol'd diffusion)} \tag{30}$$

On the other hand, if initial conditions are chosen within "islands" of stable oscillatory motion: $[\bar{Y}(m) - \bar{Y}(n)] \propto (\Delta N_1)^{-1}$, whence

$$\frac{D_2}{D_1} \propto \frac{(\Delta N_1)^3}{(\Delta N_2)^3} = 10^{-3} \qquad \text{(for oscillations)} \tag{31}$$

Placing our initial X_0, X_1 at the point A, inside the separatrix of Fig. 5a, and starting with Y_0, Y_1 selected among the values -.01, -.005, 0.0, 0.005, .01 we computed after $N = 10^6$ iterations, on the average,

$$D_1 = .72 \times 10^{-11} \quad , \quad D_2 = 0.4 \times 10^{-11}$$

or

$$D_2/D_1 = 0.6 \qquad \text{(for diffusion)} \tag{32}$$

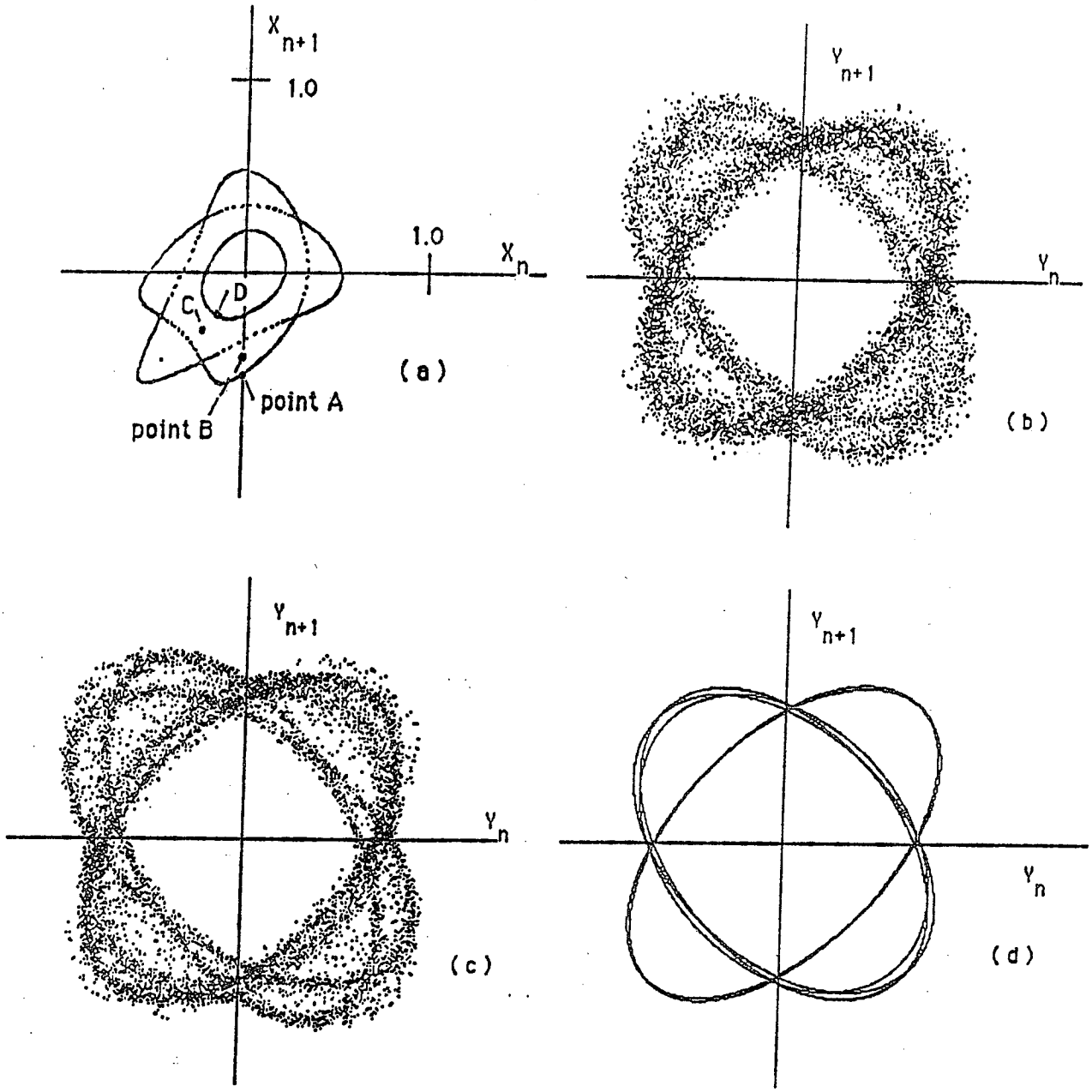

Figure 5. Evidence of weak (Arnol'd) diffusion in the Y_n (vertical) motion for $q_x = 0.21$, $q_y = 0.24$.

(a) Chaotic layer of the unstable period 5, 2–D orbit with $Y_0 = Y_1 = 0$, passing by point A: $X_0 = -.0049$, $X_1 = -.5329$.

(b) With (X_0, X_1) at A and $Y_0 = 0.0$, $Y_1 = 10^{-4}$ a diffusive outward motion in the Y_n's is observed (Magnification=8×10^5).

(c) Same as (b) with $Y_0 = 10^{-7}$, under a magnification of 8×10^8: Diffusive motion is evident, unlike:

(d) where $X_0 = -.0019$, $X_1 = -.4569$ are located at point B at the center of one of the islands of (a).

Starting, finally, with X_0, X_1 at a point B inside one of the islands of Fig. 5a and averaging over a similar set of Y_0, Y_1 initial conditions as above gives

$$D_1 = .32 \times 10^{-18} \quad , \quad D_2 = .17 \times 10^{-19} \ ,$$

and

$$D_2/D_1 = 5.3 \times 10^{-2} \qquad \text{(for oscillations)} \tag{33}$$

Thus, not only are the diffusion rates 7–8 orders of magnitude *smaller* in the oscillatory regimes, the ratio D_2/D_1 is also a lot lower than in the diffusive case (32), as expected. Eq. 33 is, of course, quite larger than predicted in (31) (and one order of magnitude higher than found by Chirikov et al. in Ref. 16). We have checked, however, our program in other oscillatory regimes, starting with X_0, X_1 at points C, D in Fig. 5a and have found results

$$\text{for point } C: \quad D_1 = 10^{-16.7} \ , \ D_2 = 10^{-18.7} \ \rightarrow \ D_2/D_1 = 10^{-2}$$
$$\text{for point } D: \quad D_1 = 10^{-16.95} \ , \ D_2 = 10^{-19.37} \ \rightarrow \ D_2/D_1 = 3.8 \times 10^{-3}$$

which are a lot closer to the expected value of Eq. 31 and clearly distinguish Eq. 32 as demonstrating the presence of a weak (Arnol'd) diffusion process.

4. Concluding Remarks

We have studied a 4–D mapping model of the dynamics of hadron beams passing repeatedly through a FODO cell containing sextupole nonlinearities (concentrated at one point), a dipole field and 2 focusing quadrupoles, in the storage ring of a high energy accelerator.

We found that low period 4–D periodic orbits of the map, when *stable*, have 3–D "tori" around them on which the orbits execute bounded oscillations for 10^6 mapping iterations and beyond. However, particles entering the large chaotic regions about such *unstable* low period orbits experience *strong instabilities* that quickly (over a few hundred iterations) lead them to *infinite* distances away from the origin of the map.

We have also discovered "tune" values (betatron frequencies) for which nearly "flat" beams ($|y_n| << |x_n|$) execute bounded oscillations (at least up to 10^7 passages through the cell) near *stable* 2–D periodic orbits of the x_n–mapping ($y_n \equiv 0$). However, when the initial x_0, x_1 are placed inside the chaotic layer of one such unstable 2–D orbit, a slow outward diffusion in the y_n motion is observed, with diffusion coefficient $D \leq 10^{-11}$ for $N = 10^6$ mapping iterations.

Comparing with the results of other researchers we have verified that this *weak instability* is indeed evidence of *Arnol'd diffusion*, which typically occurs at much faster rates than one finds when x_1, x_0 lie within oscillatory regimes ($D \leq 10^{-19}$).

These computations must, of course, be carried out for longer times ($N = 10^7$ and beyond...) and compared with analytical diffusion estimates existing in the

literature[7,16]. Moreover, synchrotron oscillations (causing a slow modulation in the q_x, q_y betatron frequencies) also need to be included in our model and their effect on beam lifetimes analyzed numerically as well as analytically[10]. Such studies are currently under way, and results will be reported in a forthcoming paper[11].

5. Acknowledgments

One of the authors (T.B.) is indebted to the organizers of this conference, and in particular to G. Turchetti, for many informative discussions on the model studied in this paper. He also gratefully acknowledges the hospitality of the Center for Statistical Mechanics and Complex Systems and the Institute of Fusion Studies of The University of Texas at Austin, where this research was carried out, while he was a visiting professor in the spring semester of 1989-90.

6. References

1. *Nonlinear Dynamics and the Beam–Beam Interaction*, M. Month and J.C. Herrera eds., A.I.P. Conf. Proc. **57** (A.I.P., New York, 1979).
2. *Physics of High Energy Accelerators*, R.A. Carrigan, F.R. Huson and M. Month eds., A.I.P. Conf. Proc. **87** (A.I.P., New York, 1982); see esp. the articles by A. Dragt and J.L. Tennyson.
3. *Proceeding of the Beam–Beam Interaction Seminar*, SLAC Publ. 2624, Conf. 8005102 (SLAC, Stanford, 1980).
4. See several articles in *Workshop on Orbital Dynamics and Applications to Accelerators*, Particle Accelerators **19** (1986).
5. See e.g. A. Bazzani, P. Mazzanti, G. Servizi and G. Turchetti, Il Nuovo Cim. **102B**(1) (1988) p. 51.
6. T. Bountis, C.R. Eminhizer and N. Budinsky, Nucl. Instr. Meth. Phys. Res. **227** (1984) p. 205.
7. B.V. Chirikov, Phys. Rep. **52** (1979) p. 265.
8. A. Ruggiero, in Ref. 4, p. 157.
9. R.H.G. Helleman in *Long Time Prediction in Dynamics*, C.W. Horton, L.E. Reichl and V. Szebehely eds. (J. Wiley, New York, 1982) p. 95.
10. F. Vivaldi, Rev. Mod. Phys. **56** (4) (1984) p. 737.
11. T. Bountis, G. Mahmoud, G. Servizi and G. Turchetti, in preparation.
12. R.H.G. Helleman in *Statistical Mechanics and Statistical Methods*, U. Landman ed. (Plenum, New York, 1978).
13. R.H.G. Helleman and T. Bountis, Lect. Notes in Phys. **93** (Springer, New York, 1978).
14. See e.g. J.E. Howard and R.S. MacKay, J. Math. Phys. **28** (1986) p. 1036; H–T. Kook and J.D. Meiss, Physica **35D** (1989) p. 65.

15. T. Bountis and R.H.G. Helleman, J. Math. Phys. **22** (9) (1981) p. 1867.
16. B.V. Chirikov, J. Ford and F. Vivaldi, in Ref. 1.